Bubble Dynamics and Gravitational Wave Spectrum from First-Order QCD Phase Transitions

Hong Mao (毛鸿)
School of Physics, Hangout Normal University

In collaboration with: Shuying Zhou, Song Shu, Wan-Ping Shen, Junrong Wang, Ziwan Yu, Jin Jinshuang, Jingdong Shao, Mei Huang and Bikai Gao

Based on works:
Shuying Zhou, Song Shu & **HM**, Chin. Phys. C **45** (2021) 043104; Shuying Zhou, Wan-Ping Shen & **HM**, Acta Phys. Sin. **71** (2022) 211101; Junrong Wang, Ziwan Yu & **HM**, Chin. Phys. C **48** (2024) 053105; Junrong Wang, Jin Jinshuang & **HM**, Symmetry **16** (2024) 893; Jingdong Shao, **HM** & Mei Huang, Phys. Rev. D **111** (2025) 023052; Chin. Phys. C **49** (2025) 065103; Bikai Gao, Jingdong Shao & **HM**, Phys. Rev. D **114** (2026) 023026.

Chirality 2026, Nov 16-20 @ Zhuhai, China

Outline

01 The Motivation

02 The Friedberg-Lee model

03 The quark-meson model

04 The Polyakov quark-meson model

05 The parity doublet model

06 The Gravitational Waves spectrum from first-order QCD transitions

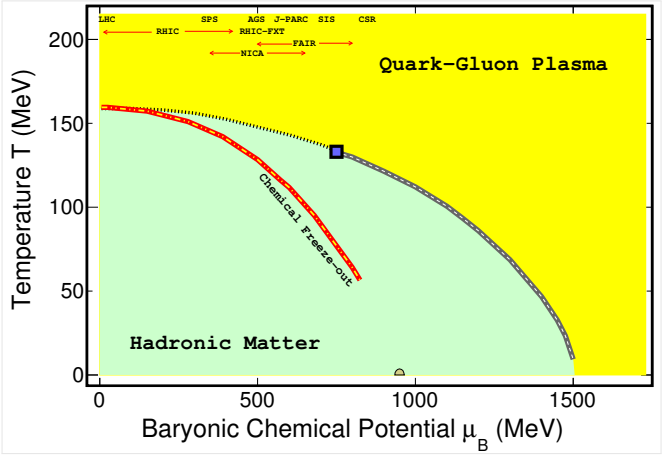
07 Summary and outlook

01

The Motivation

Why bubble dynamics and gravitational waves of a first-order QCD transition?

A conjectured QCD phase diagram



A. Pandav, D. Mallick, B. Mohanty, Prog. Part. Nucl. Phys. **125** (2022) 103960

The Motivation

1. Due to the **fermion sign problem**, an ab initio approach — Lattice Field Theory — is severely hampered by the failure of importance sampling once a chemical potential is involved.
2. After the discovery of gravitational waves by LIGO, cosmological first-order phase transitions have attracted growing interest; most works focus on the **electroweak** transition relevant to baryogenesis.
3. It is a **multimessenger era**: understanding the dynamics of the first-order quark–hadron transition and its gravitational waves is equally crucial.
4. The dynamics of first-order transitions — in the early universe and in ultrarelativistic heavy-ion collisions — is described by **homogeneous nucleation theory**. Previous studies mostly adopted the **thin-wall approximation**; we argue that a precise, exact numerical solution is essential, especially when the temperature is far from critical.

02

The Friedberg-Lee Model

A toy model in which only a first-order transition exists

2.1 The Lagrangian

The Lagrangian of the Friedberg-Lee model

$$\mathcal{L} = \bar{\psi}\,(i\partial\!\!\!/ - g\sigma)\psi + \frac{1}{2}\,\partial_\mu\sigma\,\partial^\mu\sigma - U(\sigma),$$

$$U(\sigma) = \frac{1}{2!}\,a\sigma^2 + \frac{1}{3!}\,b\sigma^3 + \frac{1}{4!}\,c\sigma^4.$$

The potential has a **local minimum** at $\sigma = 0$, and the **global minimum** at $\sigma = \sigma_v$, with

$$\sigma_v = \frac{3|b|}{2c}\left[1 + \left[1 - \frac{8ac}{3b^2}\right]^{\frac{1}{2}}\right].$$

R. Friedberg and T. D. Lee, Phys. Rev. D **15** (1977) 1694; **16** (1977) 1096; **18** (1978) 2623

2.2 The effective potential

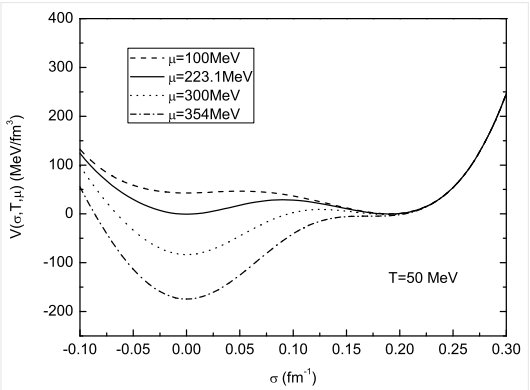
Based on thermal field theory, the one-loop finite temperature effective potential *(without the vacuum fluctuations)*

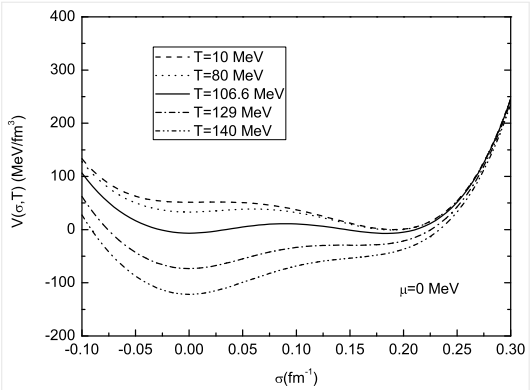
$$V_{\rm eff}(\sigma;T,\mu)=U(\sigma)+V_B(\sigma;T)+V_F(\sigma;T,\mu),$$

$$V_B(\sigma;T)=T\int\frac{{\rm d}^3p}{(2\pi)^3}\,\ln\left(1-{\rm e}^{-E_\sigma/T}\right),$$

$$V_F(\sigma;\beta,\mu)=-2N_fN_cT\int\frac{{\rm d}^3p}{(2\pi)^3}\left[\ln\left(1+{\rm e}^{-(E_q-\mu)/T}\right)+\ln\left(1+{\rm e}^{-(E_q+\mu)/T}\right)\right].$$

HM, M. Yao and W.-Q. Zhao, Phys. Rev. C **77** (2008) 065205; S. Zhou, S. Shu and **HM**, Chin. Phys. C **45** (2021) 043104





Remark

There is only a **first-order** phase transition in the FL model, so it should be taken as a **toy model**.

2.3 Homogeneous thermal nucleation

The free energy of a nucleation bubble:

The free-energy change associated with a bubble of radius R contains two competing terms:

$$\Delta F(R) = \underbrace{4\pi R^2 \Sigma_{\text{wall}}}_{\text{surface cost}} - \underbrace{\frac{4\pi}{3} R^3 \Delta f}_{\text{bulk gain}} .$$

Surface cost

Creating the interface costs energy, $\propto R^2$: big bubbles are unfavoured.

Bulk gain

Converting the volume into the true vacuum releases energy, $\propto R^3$: large bubbles grow.

For the nucleation of small bubbles, the energy cost is higher than the energy gain. Therefore, small bubbles shrink. On the other hand, a very large bubble represents a large bulk energy gain, which is higher than the surface energy cost in creating the bubble. As a consequence, large bubbles tend to grow even more and to occupy the whole system, completing the phase transition.

The critical bubble

In the field theory of bubble nucleation, a scalar field is the order parameter, and a coarse-grained free-energy functional is defined as

$$F(\sigma) = \int \mathrm{d}^3 r \left[\frac{1}{2} (\nabla \sigma)^2 + V_{\mathrm{eff}}(\sigma; T, \mu) \right].$$

The critical bubble configuration extremizes F with respect to σ:

$$\frac{\mathrm{d}^2 \sigma(r)}{\mathrm{d}r^2} + \frac{2}{r} \frac{\mathrm{d}\sigma(r)}{\mathrm{d}r} = \frac{\partial V_{\mathrm{eff}}(\sigma; T, \mu)}{\partial \sigma},$$

with boundary conditions

$$\lim_{r \to \infty} \sigma(r) = 0 \quad \text{and} \quad \frac{\mathrm{d}\sigma(0)}{\mathrm{d}r} = 0.$$

Why the thin-wall approximation?

When the system is very close to the critical coexistence line, the typical bubble radius becomes much larger than the wall thickness, and the second term in the equation of motion can be neglected:

$$\frac{\mathrm{d}^2\sigma(r)}{\mathrm{d}r^2} + \underbrace{\frac{2}{r}\frac{\mathrm{d}\sigma(r)}{\mathrm{d}r}}_{\textit{neglected}} = \frac{\partial V_{\mathrm{eff}}(\sigma; T, \mu)}{\partial \sigma}$$

$$\frac{\mathrm{d}^2\sigma(r)}{\mathrm{d}r^2} = \frac{\mathrm{d}V_{\mathrm{eff}}}{\mathrm{d}\sigma} \implies \frac{\mathrm{d}\sigma(r)}{\mathrm{d}r} = \pm\sqrt{2V_{\mathrm{eff}}} \implies r = \int_{\sigma}^{\sigma_v} \frac{\mathrm{d}\sigma}{\sqrt{2V_{\mathrm{eff}}}}.$$

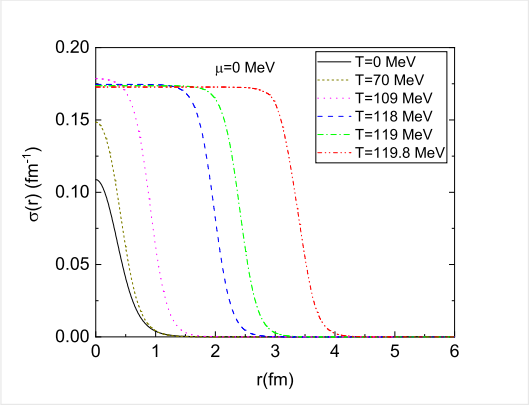
Consequences of the thin-wall approximation

$$F(R) = 4\pi R^2\Sigma - \frac{4}{3}\pi R^3\varepsilon \qquad \implies \qquad 0 = \frac{\mathrm{d}F}{\mathrm{d}R} = 8\pi R\Sigma - 4\pi R^2\varepsilon$$

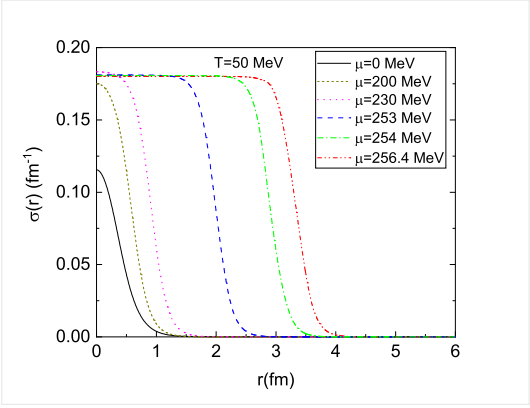
$$R_c = \frac{2\Sigma}{\varepsilon} \qquad \Sigma_{tw} = \int_0^\infty \mathrm{d}r \left[\tfrac{1}{2}\left(\tfrac{\mathrm{d}\sigma_b}{\mathrm{d}r}\right)^2 + V_{\mathrm{eff}}\right] \qquad \Delta F_b = \frac{16\pi}{3}\frac{\Sigma^3}{(\Delta V_{\mathrm{eff}})^2}$$

A. D. Linde, Nucl. Phys. B **216** (1983) 421

The critical bubble profiles



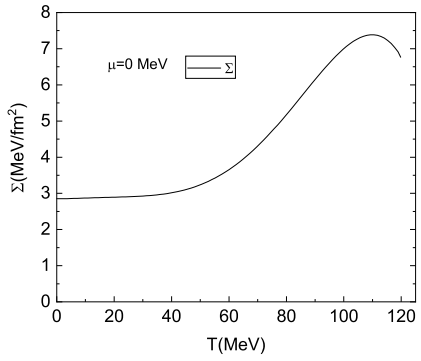
Critical bubble profiles for different temperatures at zero chemical potential.



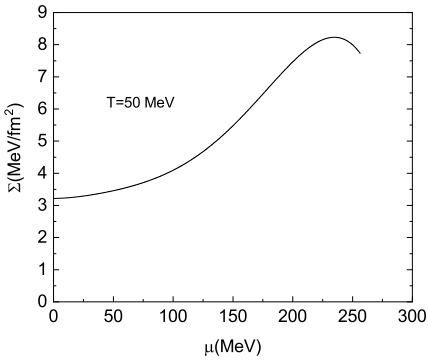
Critical bubble profiles for different chemical potentials when fixing the temperature.

S. Zhou, S. Shu and **HM**, Chin. Phys. C **45** (2021) 043104; S. Zhou, W.-P. Shen and **HM**, Acta Phys. Sin. **71** (2022) 211101

Surface tension

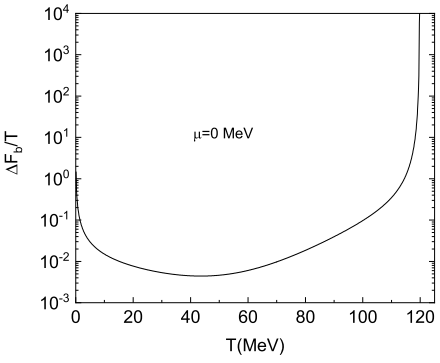


Surface tension for different temperatures at zero chemical potential.

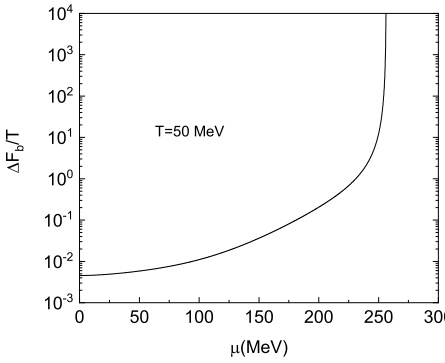


Surface tension for different chemical potentials when fixing the temperature.

The coarse-grained free energy and saddle-point action



The bubble activation free energy for different temperatures at zero chemical potential.



The bubble activation free energy for different chemical potentials when fixing the temperature.

03

The Quark–Meson Model

With chiral symmetry

3.1 The model

The Lagrangian density of the quark meson model the global $\mathrm{SU}(2)_L \times \mathrm{SU}(2)_R$ chiral phase transformations

$$\mathcal{L} = \bar{\psi}\left[i\gamma^\mu\partial_\mu - g\left(\sigma + i\gamma_5\vec{\tau}\cdot\vec{\pi}\right)\right]\psi + \frac{1}{2}\left(\partial_\mu\sigma\partial^\mu\sigma + \partial_\mu\vec{\pi}\cdot\partial^\mu\vec{\pi}\right) - U(\sigma,\vec{\pi}),$$

with the classical potential

$$U(\sigma,\vec{\pi}) = \frac{\lambda}{4}\left(\sigma^2 + \vec{\pi}^2 - v^2\right)^2 - H\sigma.$$

In mean-field approximation, the temperature-dependent effective potential **with vacuum fluctuations**

$$\Omega(T,\mu) = \frac{-T\ln\mathcal{Z}}{V} = U(\sigma,\vec{\pi}) + \Omega_{\bar{\psi}\psi},$$

$$\Omega_{\bar{\psi}\psi} = \Omega^{v}_{\bar{\psi}\psi} + \Omega^{th}_{\bar{\psi}\psi} = -\nu\int\frac{\mathrm{d}^3p}{(2\pi)^3}E - \nu T\int\frac{\mathrm{d}^3p}{(2\pi)^3}\left\{\ln\left[1+\mathrm{e}^{-(E-\mu)/T}\right] + \ln\left[1+\mathrm{e}^{-(E+\mu)/T}\right]\right\}.$$

J. Wang, Z. Yu and **HM**, Chin. Phys. C **48** (2024) 053105

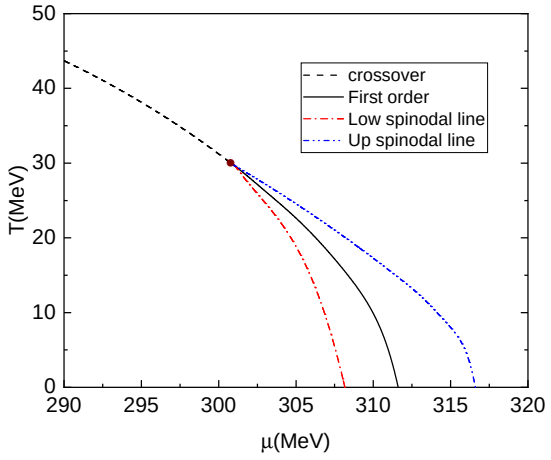
Taking into account the vacuum fluctuations and the associated renormalization, the renormalized fermion vacuum one-loop contribution reads

$$\Omega^{\mathrm{vac}}_{\bar{\psi}\psi} = \Omega^{\mathrm{reg}}_{\bar{\psi}\psi} = -\frac{N_c N_f}{8\pi^2}\, m_q^4 \ln\left(\frac{m_q}{\Lambda}\right).$$

The phase structure follows from minimizing the thermodynamic potential — **the gap equation**

$$\frac{\partial \Omega(T,\mu)}{\partial \sigma} = 0.$$

3.2 Phase diagram



- crossover line
- first-order line
- low / up spinodal lines

The critical end point is located at

$$(T_E, \mu_E) \simeq (30,\ 301)\ \mathrm{MeV}.$$

The nucleation rate

$$\Gamma = \mathcal{P} \exp\left[-\frac{S_3}{T}\right]$$

with the prefactor

$$\mathcal{P} = \frac{\omega_-}{2\pi}\left(\frac{S_3}{2\pi T}\right)^{3/2}\left[\frac{\mathrm{Det}\left(-\nabla^2 + \Omega''_{FV}\right)}{\mathrm{Det}'\left(-\nabla^2 + \Omega''_{B}\right)}\right]^{1/2}.$$

Note:
(a) ω_- is the eigenvalue of the negative mode. (b) Ω''_{FV} and Ω''_B are Ω'' in the false vacuum and in the critical bubble. (c) the prime means zero eigenvalues from translation symmetry are omitted. (d) Ω'' is the second derivative of $\Omega(T, \mu)$ with respect to σ. (e) S_3 is the three-dimensional saddle-point action of the $O(3)$-symmetric critical bubble.

A. D. Linde, Nucl. Phys. B **216** (1983) 421; **223** (1983) 544 (erratum)

The bounce

Taking the scalar field σ as the order parameter, the Euclidean action at finite temperature is

$$S_4(\sigma) = \int \mathrm{d}\tau\, \mathrm{d}^3x \left[\frac{1}{2} \left(\frac{\partial \sigma}{\partial \tau} \right)^2 + \frac{1}{2} (\nabla \sigma)^2 + \Omega(\sigma; T, \mu) \right].$$

For sufficiently high temperature,

$$\frac{S_4}{T} \simeq \frac{S_3}{T}, \qquad S_3 = \int \mathrm{d}^3x \left[\frac{1}{2} (\nabla \sigma)^2 + \Omega(\sigma; T, \mu) \right].$$

The bounce is the $O(3)$-symmetric solution extremizing S_3:

$$\frac{\mathrm{d}^2\sigma(r)}{\mathrm{d}r^2} + \frac{2}{r} \frac{\mathrm{d}\sigma(r)}{\mathrm{d}r} = \frac{\partial \Omega(\sigma; T, \mu)}{\partial \sigma}, \qquad \lim_{r \to \infty} \sigma(r) = \sigma_{FV}, \qquad \left. \frac{\mathrm{d}\sigma(r)}{\mathrm{d}r} \right|_{r=0} = 0.$$

Once σ_b is obtained, the S_3 exponent in the presence of the bounce is

$$S_3 = \int \mathrm{d}^3r \left[\frac{1}{2} (\nabla \sigma)^2 + \Omega(\sigma; T, \mu) \right],$$

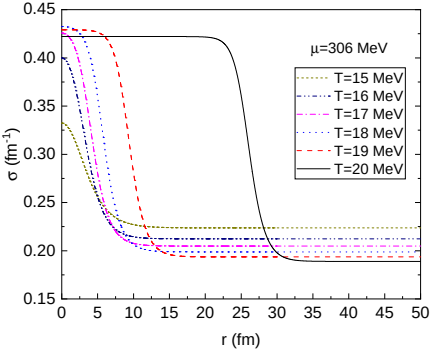
and the surface tension of the interface between the false and the true vacuum is

$$\Sigma = \int \mathrm{d}r \left[\frac{1}{2} \left(\frac{\mathrm{d}\sigma}{\mathrm{d}r} \right)^2 + \Omega(\sigma; T, \mu) \right].$$

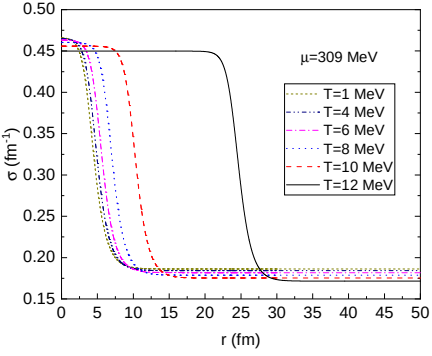
3.4 Results

The top-down scenario ($T < T_c$)

At $T \simeq T_c$, the false vacuum is the **quark phase**, with boundary conditions $\sigma \to \sigma_l$ as $r \to \infty$ and $\mathrm{d}\sigma(0)/\mathrm{d}r = 0$.

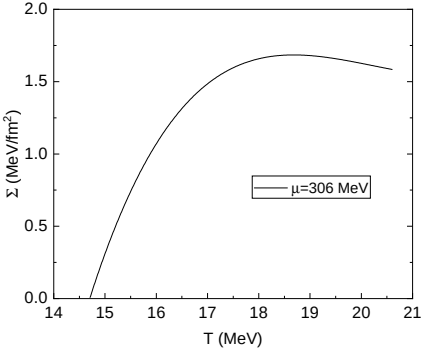


Critical bubble profiles for different temperatures at $\mu = 306$ MeV.

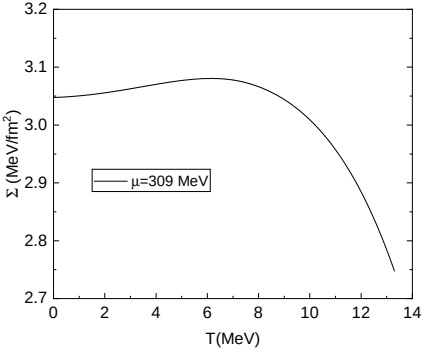


Critical bubble profiles for different temperatures at $\mu = 309$ MeV.

Surface tension ($T < T_c$)

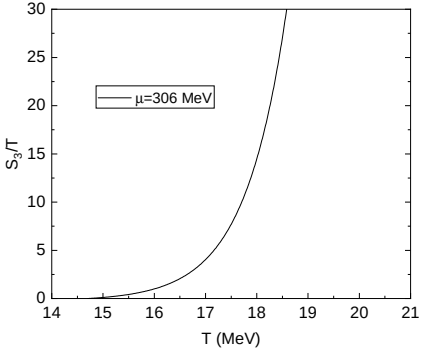


Surface tension for different temperatures at $\mu = 306$ MeV.

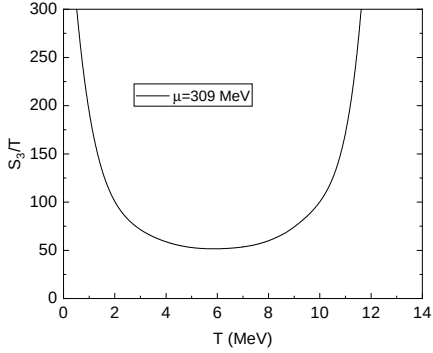


Surface tension for different temperatures at $\mu = 309$ MeV.

The saddle-point action ($T < T_c$)



The saddle-point action for different temperatures at $\mu = 306$ MeV.



The saddle-point action for different temperatures at $\mu = 309$ MeV.

04

The Polyakov Quark–Meson Model

Including the gluonic degrees of freedom

4.1 The PQM model

The Lagrangian density of the Polyakov quark-meson model

$$\mathcal{L} = \bar{\psi}\left[i\gamma^\mu\partial_\mu - g\left(\sigma + i\gamma_5\vec{\tau}\cdot\vec{\pi}\right)\right]\psi + \frac{1}{2}\left(\partial_\mu\sigma\partial^\mu\sigma + \partial_\mu\vec{\pi}\cdot\partial^\mu\vec{\pi}\right) - U(\sigma,\vec{\pi}),$$

$$U(\sigma,\vec{\pi}) = \frac{\lambda}{4}\left(\sigma^2 + \vec{\pi}^2 - v^2\right)^2 - H\sigma.$$

To include the gluonic degrees of freedom

$$D_\mu = \partial_\mu - iA_\mu, \qquad A_\mu = \delta_{\mu 0}A_0,$$

and the Polyakov loop operator is defined as

$$L(\vec{x}) = \mathcal{P}\exp\left[i\int_0^\beta \mathrm{d}\tau\, A_4(\vec{x},\tau)\right].$$

The color-traced Polyakov loops (order parameters for deconfinement) are

$$\Phi = (\mathrm{Tr}_c L)/N_c, \qquad \Phi^* = (\mathrm{Tr}_c L^\dagger)/N_c.$$

J. Wang, J. Jinshuang and **HM**, Symmetry **16** (2024) 893

The Polyakov-loop potential

A phenomenological potential $U(\Phi, \Phi^*, T)$ is constructed to reproduce lattice QCD thermodynamics, on a set of criteria:

1. invariant under the $\mathbb{Z}(3)$ center symmetry;
2. symmetric under exchange of Φ and Φ^*;
3. $\langle\Phi\rangle = \langle\Phi^*\rangle = 0$ at low T, and finite at high T.

The simplest polynomial potential from a Ginzburg–Landau ansatz:

$$\frac{\mathcal{U}(\Phi, \Phi^*, T)}{T^4} = -\frac{b_2(T)}{4}\left(|\Phi|^2 + |\Phi^*|^2\right) - \frac{b_3}{6}\left(\Phi^3 + \Phi^{*3}\right) + \frac{b_4}{16}\left(|\Phi|^2 + |\Phi^*|^2\right)^2,$$

$$b_2(T) = a_0 + a_1\left(\frac{T_0}{T}\right) + a_2\left(\frac{T_0}{T}\right)^2 + a_3\left(\frac{T_0}{T}\right)^3,$$

$$a_0 = 6.75, \quad a_1 = -1.95, \quad a_2 = 2.625, \quad a_3 = -7.44, \quad b_3 = 0.75, \quad b_4 = 7.5,$$

with $T_0 = 208$ MeV for two quark flavors.

C. Ratti, M. A. Thaler and W. Weise, Phys. Rev. D **73** (2006) 014019

4.2 The effective potential

The thermodynamic grand potential for the PQM model

$$\Omega_{\rm MF}(T,\mu) = U(\sigma,\vec{\pi}) + \mathcal{U}(\Phi,\Phi^*,T) + \Omega_{\bar{\psi}\psi},$$

$$\Omega_{\bar{\psi}\psi} = \Omega^{\rm vac}_{\bar{\psi}\psi} + \Omega^{\rm th}_{\bar{\psi}\psi} = -2N_f N_c \int \frac{{\rm d}^3p}{(2\pi)^3} E_q - 2N_f T \int \frac{{\rm d}^3p}{(2\pi)^3} \left[\ln g_q^+ + \ln g_q^-\right],$$

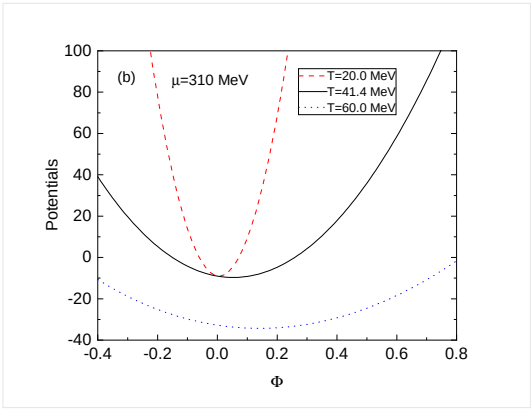
$$g_q^+ = \left[1 + 3\left(\Phi + \Phi^* {\rm e}^{-(E_q-\mu)/T}\right) \times {\rm e}^{-(E_q-\mu)/T} + {\rm e}^{-3(E_q-\mu)/T}\right],$$
$$g_q^- = \left[1 + 3\left(\Phi^* + \Phi\, {\rm e}^{-(E_q+\mu)/T}\right) \times {\rm e}^{-(E_q+\mu)/T} + {\rm e}^{-3(E_q+\mu)/T}\right],$$

$$\Omega^{\rm vac}_{\bar{\psi}\psi} = \Omega^{\rm reg}_{\bar{\psi}\psi} = -\frac{N_c N_f}{8\pi^2}\, m_q^4 \ln\left(\frac{m_q}{\Lambda}\right).$$

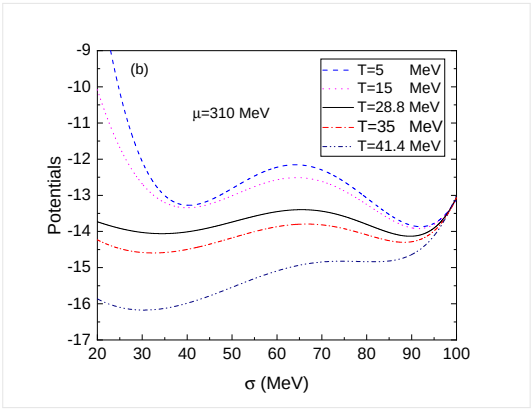
The gap equations:

$$\frac{\partial\Omega_{\rm MF}}{\partial\sigma_v} = 0, \qquad \frac{\partial\Omega_{\rm MF}}{\partial\Phi} = 0, \qquad \frac{\partial\Omega_{\rm MF}}{\partial\Phi^*} = 0.$$

The effective potential are separated into two directions

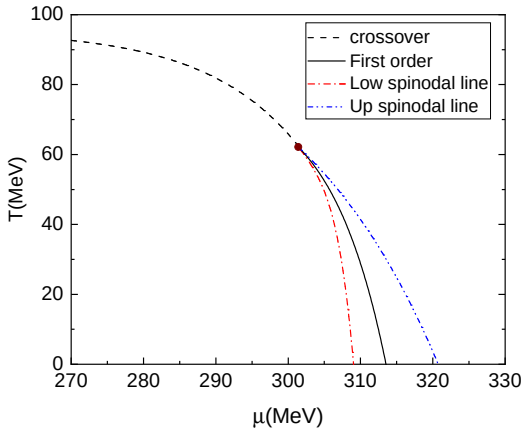


(a) the Polyakov loop filed direction:
the Polyakov loop fields are consider as variables when the σ field will maintain their expectation value all the time.



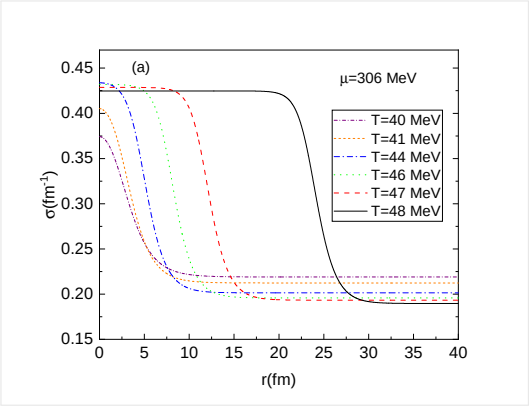
(b) the mesonic field direction:
we treat the σ field as a variable in the grand canonical potential while fixing the Polyakov loop fields on their expectation values.

4.3 Phase diagram in the first-order region

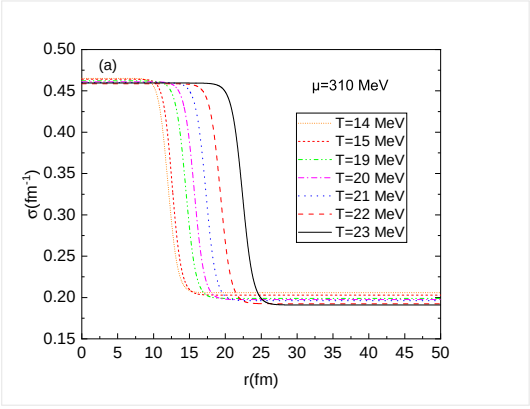


The first-order region obtained from the effective potentials, with the low and up spinodal lines bounding the metastable window.

The top-down scenario ($T < T_c$)



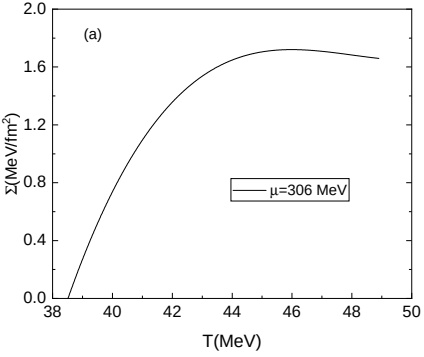
Critical bubble profiles for different temperatures at $\mu = 306$ MeV.



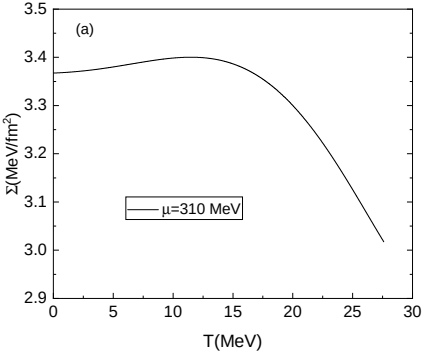
Critical bubble profiles for different temperatures at $\mu = 310$ MeV.

J. Wang, J. Jinshuang and **HM**, Symmetry **16** (2024) 893

Surface tension ($T < T_c$)

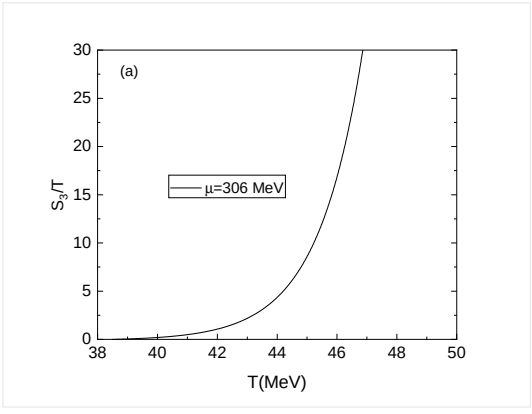


Surface tension for different temperatures at $\mu = 306$ MeV.

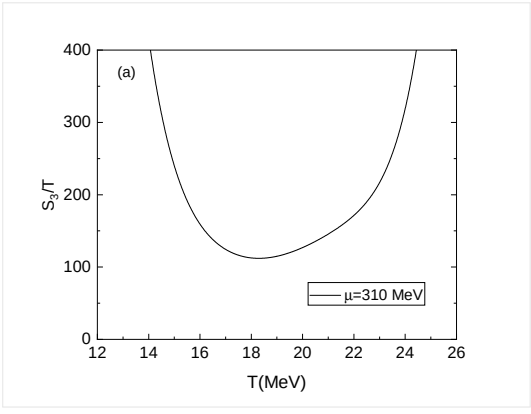


Surface tension for different temperatures at $\mu = 310$ MeV.

The saddle-point action ($T < T_c$)



The saddle-point action for different temperatures at $\mu = 306$ MeV.



The saddle-point action for different temperatures at $\mu = 310$ MeV.

05

The Parity Doublet Model

Chiral symmetry restoration with a finite invariant mass

5.1 The parity doublet model

1. Start with two massless Dirac spinors ψ_a and ψ_b of opposite parities, with ψ_a having positive parity.
2. Under a chiral transformation of $\mathrm{SU}(2)_L \times \mathrm{SU}(2)_R$,

$$\psi_a \to \mathrm{e}^{i\frac{\vec{\alpha}\cdot\vec{\tau}}{2}\gamma^5}\psi_a, \qquad \psi_b \to \mathrm{e}^{-i\frac{\vec{\alpha}\cdot\vec{\tau}}{2}\gamma^5}\psi_b.$$

3. A mass term of the following form is allowed in the Lagrangian while preserving chiral symmetry:

$$-m_0\left(\bar{\psi}_a\gamma^5\psi_b - \bar{\psi}_b\gamma^5\psi_a\right).$$

4. The fermion Lagrangian takes the form

$$\mathcal{L}_f = \bar{\psi}_a\left(i\partial\!\!\!/ - y_a(\sigma + i\gamma^5\vec{\tau}\cdot\vec{\pi})\right)\psi_a + \bar{\psi}_b\left(i\partial\!\!\!/ - y_b(\sigma - i\gamma^5\vec{\tau}\cdot\vec{\pi})\right)\psi_b - m_0\left(\bar{\psi}_a\gamma^5\psi_b - \bar{\psi}_b\gamma^5\psi_a\right).$$

C. DeTar and T. Kunihiro, Phys. Rev. D **39** (1989) 2805; B. Gao, J. Shao and **HM**, Phys. Rev. D **114** (2026) 023026

Under an orthogonal transformation

$$\begin{pmatrix}\psi_+\\ \psi_-\end{pmatrix} = \begin{pmatrix}\cos\theta & \gamma^5\sin\theta\\ -\gamma^5\sin\theta & \cos\theta\end{pmatrix}\begin{pmatrix}\psi_a\\ \psi_b\end{pmatrix},$$

the masses of ψ_+ and ψ_- are given by

$$M_\pm = \frac{1}{2}\left[\pm\sigma\left(y_a - y_b\right) + \sqrt{\sigma^2\left(y_a + y_b\right)^2 + 4m_0^2}\right].$$

The fields $\psi_\pm$ are the physical states, identified with the nucleon $N(939)$ and its parity partner $N^*(1535)$. For vanishing σ the masses of the doublet members are degenerate at the value m_0, an invariant mass.

An interesting feature: the two nucleons become degenerate with a finite mass m_0 when chiral symmetry is restored!

5.2 The thermodynamic potential

In the mean-field approximation, the effective potential is given by

$$\Omega = \Omega_H + V(\sigma) - V_0(\sigma) + V_\omega,$$

with

$$\Omega_H = -2T \sum_{\alpha=\pm} \sum_{i=p,n} \int \frac{\mathrm{d}^3 p}{(2\pi)^3} \left[\ln\left(1 - f_{\alpha,i}\right) + \ln\left(1 - \bar{f}_{\alpha,i}\right) \right],$$

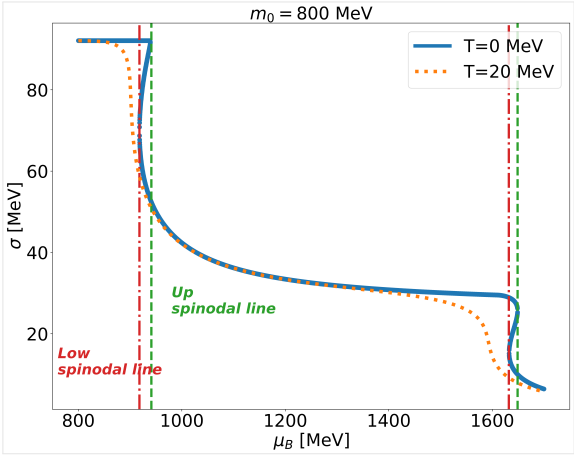
$$\begin{aligned} V(\sigma) &= -\frac{1}{2}\bar{\mu}^2\sigma^2 + \frac{1}{4}\lambda\sigma^4 - \frac{1}{6}\lambda_6\sigma^6 - m_\pi^2 f_\pi \sigma, \\ V_0(\sigma) &= -\frac{1}{2}\bar{\mu}^2 f_\pi^2 + \frac{1}{4}\lambda f_\pi^4 - \frac{1}{6}\lambda_6 f_\pi^6 - m_\pi^2 f_\pi^2, \\ V_\omega &= -\frac{1}{2} m_\omega^2 \omega^2. \end{aligned}$$

Y. Motohiro, Y. Kim and M. Harada, Phys. Rev. C **92** (2015) 025201; **95** (2017) 059903(E)

The mean fields σ, ω follow from the gap equations

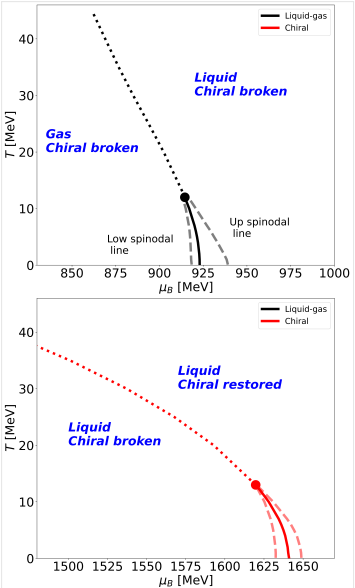
$$\frac{\partial \Omega}{\partial \sigma} = 0, \qquad \frac{\partial \Omega}{\partial \omega} = 0.$$

At $T = 0$ the chiral transition and the liquid–gas transition coexist; the up spinodal line ends at the critical point of the liquid–gas transition.



$\langle \sigma \rangle$ as a function of μ_B for $T = 0$ and 20 MeV

5.3 Phase diagram



5.4 Homogeneous thermal nucleation

The nucleation rate per unit volume is

$$\Gamma(t) = A(t)\, \mathrm{e}^{-S_4(t)},$$

where S_4 is the four-dimensional Euclidean action on the $O(4)$-symmetric bounce, and the prefactor reads

$$A(T) = T^4 \left(\frac{S_3}{2\pi T}\right)^{3/2}.$$

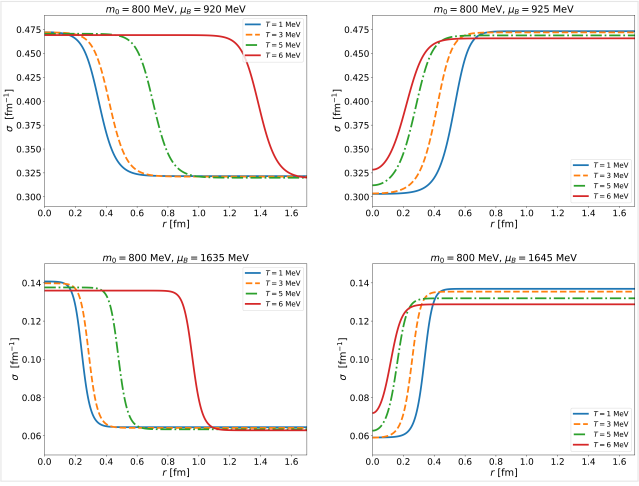
The three-dimensional action is obtained by evaluating the energy functional on the bounce,

$$S_3 = \int \mathrm{d}^3 r \left[\frac{1}{2}(\nabla\sigma)^2 + \Delta\Omega(\sigma, T, \mu_B)\right].$$

Assuming spherical symmetry, the bounce satisfies

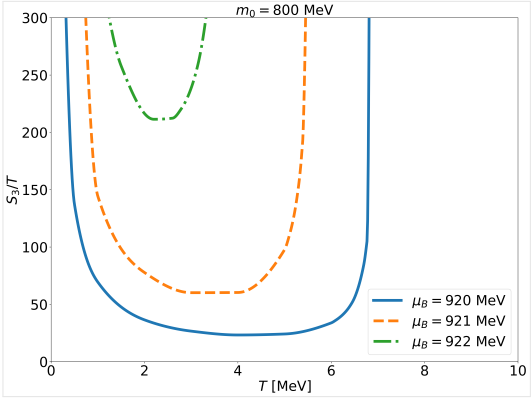
$$\frac{\mathrm{d}^2\sigma(r)}{\mathrm{d}r^2} + \frac{2}{r}\frac{\mathrm{d}\sigma(r)}{\mathrm{d}r} = \frac{\partial\Omega(\sigma, T, \mu_B)}{\partial\sigma}, \qquad \lim_{r\to\infty}\sigma(r) = \sigma_{FV}, \quad \left.\frac{\mathrm{d}\sigma(r)}{\mathrm{d}r}\right|_{r=0} = 0.$$

Bounce profiles

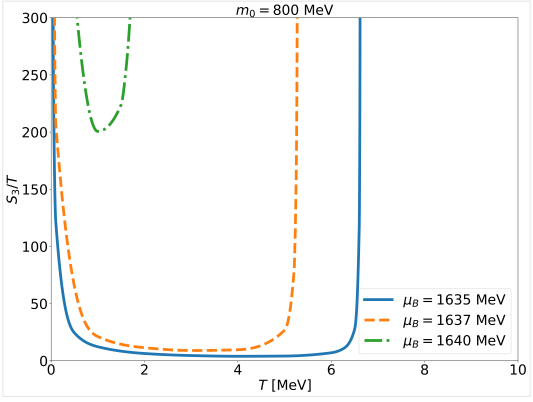


Bounce profiles of the chiral mean field $\sigma(r)$ as a function of the radial coordinate r, for $m_0 = 800$ MeV and $T = 1, 3, 5, 6$ MeV.

S_3/T near the two transitions



liquid–gas transition



chiral transition

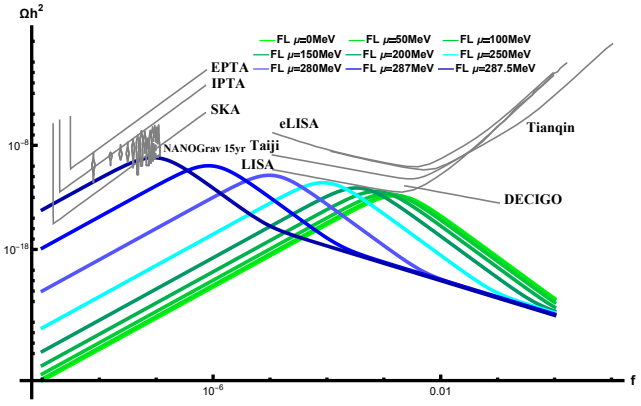
S_3/T as a function of T for several values of μ_B

06

Gravitational Waves

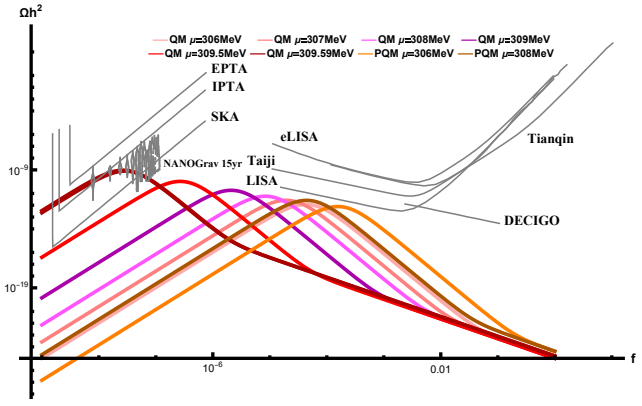
From the nucleation rate to the stochastic background

6.1 Gravitational Wave spectra in the FL model



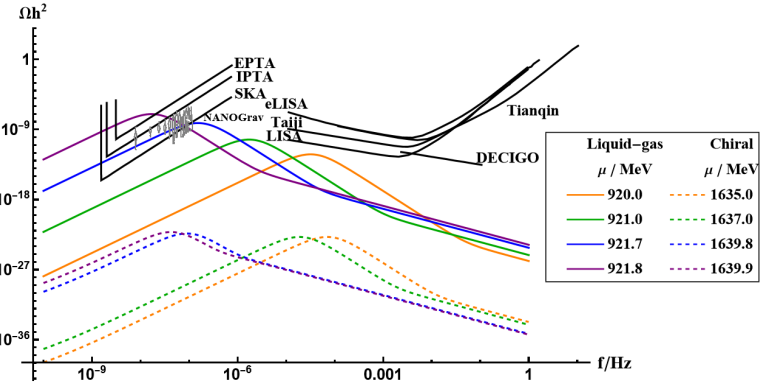
J. Shao, **HM** and M. Huang, Phys. Rev. D **111** (2025) 023052; Chin. Phys. C **49** (2025) 065103

6.2 Gravitational Wave spectra in the QM and PQM models



J. Shao, **HM** and M. Huang, Phys. Rev. D **111** (2025) 023052; Chin. Phys. C **49** (2025) 065103

6.3 Gravitational Wave spectra from the liquid–gas and chiral transitions



Solid curves: liquid–gas transition; dashed curves: chiral transition

B. Gao, J. Shao and **HM**, Phys. Rev. D **114** (2026) 023026

07

Summary and Outlook

What we have learned and where we go next

Summary

1. We investigate the **dynamics** of a first-order quark-hadron transition and the possible **GW spectra** via homogeneous thermal nucleation, in the quark-meson model with and without the Polyakov loop, and in the parity doublet model.
2. Taking temperature as the variable, the critical bubble profiles, the evolution of the surface tension and of S_3/T are computed **numerically** in detail.
3. For chiral effective models, the false vacuum can **survive** as a metastable state as long as T lies between the low and up spinodal lines.
4. The effective models predict a surface tension $\Sigma \sim$ 0-10 $\mathrm{MeV/fm^2}$; such a small value would favor a **mixed phase** in the cores of compact stars.

Future studies

1. Apply our studies to other effective models, such as a **chiral nucleon-meson model** or a quark-meson model with **scale symmetry**.
2. Extend the work to the **3-flavor** quark-meson model with and without the Polyakov loop, and to the parity doublet model including the strange quark.
3. For the physics of interest here, **the prefactor** can be estimated as T^4 by dimensional analysis. However, when T approaches the spinodal lines, $S_3/T < 1$ and the rate is dominated by the prefactor – calculations of **functional determinants** are under consideration.

Thank you!